The Helical Structure of Surfactant Peptide KL_4 When Bound to POPC: POPG Lipid Vesicles[†]

Frank D. Mills, Vijay C. Antharam, Omjoy K. Ganesh, Doug W. Elliott, Seth A. McNeill, and Joanna R. Long*

Department of Biochemistry and Molecular Biology and McKnight Brain Institute, University of Florida, Box 100245, Gainesville, Florida 32610-0245

Received December 31, 2007; Revised Manuscript Received June 6, 2008

ABSTRACT: KL_4 is a 21-residue peptide employed as a functional mimic of lung surfactant protein B, which successfully lowers surface tension in the alveoli. A mechanistic understanding of how KL_4 affects lipid properties has proven elusive as the secondary structure of KL_4 in lipid preparations has not been determined at high resolution. The sequence of KL_4 is based on the C-terminus of SP-B, a naturally occurring helical protein that binds to lipid interfaces. The spacing of the lysine residues in KL_4 precludes the formation of a canonical amphipathic α-helix; qualitative measurements using Raman, CD, and FTIR spectroscopies have given conflicting results as to the secondary structure of the peptide as well as its orientation in the lipid environment. Here, we present a structural model of KL_4 bound to lipid bilayers based on solid state NMR data. Double-quantum correlation experiments employing ^{13}C-enriched peptides were used to quantitatively determine the backbone torsion angles in KL_4 at several positions. These measurements, coupled with CD experiments, verify the helical nature of KL_4 when bound to lipids, with (ϕ, ψ) angles that differ substantially from common values for α-helices of (−60, −45). The average torsion angles found for KL_4 bound to POPC:POPG lipid vesicles are (−105, −30); this deviation from ideal α-helical structure allows KL_4 to form an amphipathic helix at the lipid interface.

Pulmonary surfactant is a lipid-rich fluid, containing key proteins, forming the inner mucosal lining of the alveoli. The primary functions of lung surfactant are to minimize surface tension at the alveolar air−fluid interface and provide a barrier against disease (*1–5*). Inadequate protein levels are a leading cause of respiratory distress syndrome (RDS[1]) in premature infants (*6–8*). Current therapies for RDS primarily rely on administration of lung surfactant from exogenous sources (*9–12*). This reliance on xenogenic surfactant is due to the critical role of lung surfactant protein B (SP-B), a highly hydrophobic, 79 residue protein which functions as a homodimer containing 7 disulfide bridges (*13*). A multitude of roles for SP-B have been proposed and experimentally established. These include surface tension minimization, facilitation of lipid adsorption and resorption at the air−fluid interface, intracellular surfactant trafficking and improved respiratory dynamics in general (*14*).

Synthetic, peptide-based lung surfactant replacements have received noticeable attention (*15–17*) as the use of synthetic analogs would remove the immunologic risks associated with animal-derived surfactant and allow for greater therapeutic consistency (*12, 15*). The twenty-one amino acid residue peptide KL_4, KLLLLKLLLLKLLLLKLLLLK, was designed based on the periodic hydrophobicity of the C-terminus of SP-B and has shown promise in the relief of respiratory distress syndrome (*18*). Molecular level information on how synthetic peptides, unrelated at the amino acid level to SP-B, can modulate surface tension in alveolar compartments is lacking, yet KL_4, in combination with lipids found in lung surfactant and palmitic acid, has been approved for treatment of RDS due to its efficacy (*12, 19–22*). *In-vitro* assays as well as animal studies have shown the ability of KL_4 to lower surface tension in different lipid systems (*18, 23*). Clinical studies show administration to very premature infants of a KL_4 surfactant preparation (lucinactant) was markedly more effective than other commercially available formulations (*24*). Thus, understanding how KL_4 affects the molecular and biophysical properties of the lipids is of particular relevance to the treatment of various forms of RDS.

The structure of KL_4 in a lipid milieu similar to the lung surfactant environment has not been conclusively determined. While SP-B has been shown by CD and FTIR measurements to form a helical protein at membrane interfaces (*25–27*), the spacing of the cationic lysines in KL_4 rule out a structural model in which the peptide binds to lipid interfaces as a classic, amphipathic α-helix. Several studies using various spectroscopies have attempted to determine the structure and orientation of KL_4 in lipid bilayers, but they have yielded conflicting interpretations regarding both the secondary structure of KL_4 as well as its orientation in a lipid environment. Initial characterization of KL_4 by fluorescence

[†] This work was supported by a National Institutes of Health Grant HL-076586 (to J.R.L.) and by the University of Florida (startup funds to J.R.L.). NMR experiments were performed in the Advanced Magnetic Resonance Imaging and Spectroscopy Facility which is supported by an NSF grant to the National High Magnetic Field Laboratory.

* To whom correspondence should be addressed. Tel: 352-846-1506. Fax: 352-392-3422. E-mail:jrlong@mbi.ufl.edu

[1] Abbreviations: RDS, respiratory distress syndrome; SP-B, surfactant protein B; ssNMR, solid state nuclear magnetic resonance; MLV, multilamellar vesicle; LUV, large unilamellar vesicle; POPC, 1-palmitoyl-2-oleoyl-*sn*-glycero-3-phosphatidylcholine; POPG, 1-palmitoyl-2-oleoyl-*sn*-glycero-3-phosphatidylglycerol; P/L, peptide/lipid molar ratio; CD, circular dichroism.

10.1021/bi702551c CCC: $40.75
Published on Web 07/18/2008

emission spectroscopy, using peptide analogs incorporating tryptophan, suggested KL_4 partitions at the membrane interface (*18*). Using ATR-IR and CD characterization, Gustafsson et al. concluded that while KL_4 may be helical, with an amide I′ band at 1657 cm^{-1}, it spans 1,2- dipalmitoyl-phosphatidylcholine (DPPC)/phosphatidylglycerol (PG) bilayers (*28*). This conclusion was drawn based on a comparison of spectra collected with parallel and perpendicular polarized incident light with respect to the normal of the sample germanium plate and assuming the lipid bilayers orient on the surface of this ATR plate. In contrast, Cai et al., using IR refection-absorption spectroscopy at an air−water interface, observed amide I′ bands 1652 and 1620 cm^{-1}, and correlated them to α-helix and an extended structure, respectively (*29*). Based on the growth of the lower wavenumber band at high surface pressures, they concluded KL_4 assumes an extended conformation in DPPC and DPPC/1, 2- dipalmitoyl- phosphatidylglycerol (DPPG) lipid monolayers. However, they observed predominantly a helical form of KL_4 in DPPG monolayers. Some of this divergence between studies may be due to differences in sample preparation and experimental configuration. A recent investigation utilizing CD to study the effect of peptide:lipid ratios and lipid composition on the structure of KL_4 suggests a helical secondary structure is highly dependent on the presence of negatively charged lipids, such as PG, and fluidity of the membrane (*30*). Unsaturated lipids decrease bilayer packing density and favor the helical conformation. However, the analysis and deconvolution of the data obtained to date using CD and IR spectroscopies is dependent on the assumption of canonical secondary structures that may provide an inconsistent classification of the peptide's secondary structure. Additionally, the amide I′ band in FTIR spectroscopy is particularly sensitive to the solvation state of the peptide backbone (*31*), which is dependent on the insertion depth of the peptide as well as side chain conformations. More fundamentally, these studies do not address how KL_4, with its atypical charge distribution, is able to adopt either a helical or sheet-like structure when bound at lipid interfaces.

The study presented here examines the structure of KL_4 in a model lipid system similar to the composition of lung surfactant using solid state nuclear magnetic resonance (ssNMR) dipolar recoupling techniques. By selective isotopic labeling during peptide synthesis, we are able to probe the structure and dynamics at specific residues in KL_4 by ssNMR, allowing high resolution measurements. Understanding the structure and dynamics of KL_4 in lipid environments at a fundamental, molecular level will provide us with insights into its functional properties and allow further development of effective treatments for respiratory distress syndrome. Thus, we utilized a suite of circular dichroism and magic angle spinning (MAS) ssNMR experiments to explore the behavior of KL_4 on binding to lipid vesicles as well as dipolar recoupling ssNMR techniques to directly determine the backbone (ϕ, ψ) torsion angles in KL_4 at several positions.

MATERIALS AND METHODS

Synthesis of KL_4. Isotopically enriched Fmoc amino acids were synthesized starting with $^{13}C'$-enriched amino acids (Cambridge Isotope Laboratories, Inc.) and using standard protocols (*32*). KL_4 (KLLLLKLLLLKLLLLKLLLLK) was synthesized via automated solid-phase peptide synthesis on a Wang resin (ABI 430, ICBR, University of Florida). The peptide was cleaved from the resin with 90% TFA/5% triisopropyl-silane/5% water and ether precipitated. The crude product was purified by RP-HPLC using an acetonitrile/water gradient and purity was verified by mass spectrometry.

Preparation of KL_4 in Buffer. Dried peptide was weighed and dissolved in methanol to ensure full dissociation prior to addition of water. The solution of 1:1 methanol: water was then placed under a stream of compressed nitrogen gas to remove the methanol and 100 mM HEPES buffer was added to achieve a final concentration of <100 μM of KL_4 in 5 mM HEPES, pH 7.4.

Preparation of 3:1 POPC:POPG LUVs. 1-Palmitoyl-2-oleoyl-phosphaticylcholine (POPC) and 1-palmitoyl-2-oleoyl-phosphaticylglycerol (POPG) were purchased (Avanti Polar Lipids, Alabaster, AL) as chloroform solutions. The lipids were mixed at a molar ratio of 3:1 POPC:POPG and the $CHCl_3$ was removed under N_2. The dried lipid film was dissolved in cyclohexane and lyophilized to remove residual chloroform. The lipids were then reconstituted in 5 mM HEPES at pH 7.4 and subjected to 3 to 5 freeze−thaw cycles to facilitate the formation of multilamellar vesicles (MLVs). Large unilamellar vesicles (LUVs) were prepared by extrusion of the MLVs through 100 nm polycarbonate filters (Avanti Polar Lipids) (*33*).

Preparation of CD Samples and Collection of CD Spectra. Stock solutions of KL_4 in buffer (40−80 μM) were mixed with lipid vesicles at peptide:lipid ratios of 1:200, 1:100, 1:60 and 1:35. The peptide−lipid mixtures were equilibrated for at least an hour before acquiring spectra. The final concentration of peptide in the samples was 20−40 μM and the final concentration of lipid was 1.33− 4mM. CD experiments were performed on an Aviv Model 215 at a wavelength range 195−260nm with a step size of 1 nm for 10−50 scans. Control spectra of 40 μM KL_4 in either buffer or buffer containing 50% trifluoroethanol (TFE) by volume were also collected.

Solid State NMR Sample Preparation. For each sample, a solution of ^{13}C-enriched KL_4 in buffer was added to a suspension of lipid LUVs at a molar ration of ∼1:33 to 1:100 peptide:lipid. After binding of >4 h, the lipid suspension was pelleted by ultracentrifugation. For initial NMR measurements, the pellets were packed directly into MAS rotors and chemical shift spectra were collected at room temperature. For later samples, the pellets were flash frozen in cold isopentane and lyophilized prior to being packed into MAS rotors. Samples consisted of approximately 20 mg of the lipid-peptide mixture for the pelleted samples and closer to 40 mg of peptide−lipid mixture for the lyophilized samples.

SSNMR Studies. All experiments were performed on a 500 MHz Bruker DRX system (Billerica, MA) using a doubly tuned 4 mm magic angle spinning probe (Doty Scientific; Columbia, South Carolina). Spectra were collected at room temperature and −20 °C. Cross-polarization magic angle spinning (CPMAS) experiments employed a ^1H 90° pulse width of 3.2 μs followed by a contact time of 2 ms and 110 kHz ^1H CW decoupling. A 25% ramp was applied on the ^1H channel during cross polarization. Spectra were acquired at spinning speeds of 3−5 kHz with a total of 512−2048 scans for each spectrum. The rotor speed was regulated to

± 3 Hz for all MAS experiments, and, to ensure high homogeneity in the applied radiofrequency field, samples were confined to the innermost 5 mm of the rotor. Each transient was collected with a sweep width of 50 kHz and 20 msec of acquisition (1024 points).

For the double quantum (DQ)-DRAWS experiments (*34–36*), a 42.5 kHz ^{13}C field was utilized with 110 kHz ^{1}H decoupling and the rotor frequency was set such that the rotor period equaled 8.5 ^{13}C radiofrequency periods, or 200 μs (5 kHz MAS). The DQ buildup experiments were performed with 1−2k transients per point, and for the 2D-DQ experiments 40 spectra (2k transients per spectrum) were collected over the course of one rotor period in t_1 using States-Haberkorn-Ruben phase sensitive detection. A pulse sequence diagram and phase cycling information for these experiments are included in the Supporting Information. Signal intensities were determined by integrating the isotropic carbonyl resonances and their attendant spinning sidebands.

Data Analysis. Principal values of the chemical shift tensors of the $^{13}C'$ spins for each enriched position on the peptide were determined from CPMAS spectra collected at 3, 4, and 5 kHz sample spinning and were similar to values calculated based on their isotropic chemical shifts. These principal values were then used in the simulations of the corresponding DQ experiments for each sample.

Distances between adjacent $^{13}C'$ spins were determined by a least-squares fit of DQ buildup curves to numerical simulations. In these simulations, the single quantum relaxation values were held at 50 Hz based on an independent measurement of the typical carbonyl carbon T_2 for the conditions used in these experiments. The only parameter varied in the simulations was the ϕ torsion angle, which assumed to be negative, leading to a corresponding change in the distance (and dipolar coupling) between the two atoms and their relative chemical shift anisotropies (CSAs—see comments below regarding iterative fitting). Canonical values of peptide bond lengths, bond angles, and orientations of the $^{13}C'$ CSAs relative to their respective amide planes were used to calculate the effects of changes in ϕ on the distance and CSA orientations (*37–40*).

To fit the 2D-DQ experiments, relative orientations between $^{13}C'$ CSAs as well as with the dipolar coupling interaction were calculated by orienting each individual $^{13}C'$ CSA relative to its respective amide bond, setting the ω torsion angle to 180°, varying the ϕ torsion angle ± 15° in 5° increments from the value obtained by fitting the DQ buildup data, and varying the ψ angle in 2° increments over the accessible space (180° to −180°). Numerical simulations of the 2D DQ evolution for each set of torsion angles were compared to experimental data. Relative χ^2 values were determined as described by Gabrys et al. (*41*) Chi-squared maps were generated using both a point by point comparison in t_1 and by comparing the amplitudes of the Fourier components (which are increments of the spinning speed) for the experimental and simulated t_1 data and these maps are provided in the supplementary data. The second derivative of the chi-squared map with ϕ held at the value determined by the DQ buildup experiment was used to determine the best fit and standard deviation for the ψ torsion angles at χ^2 minima.

Computer Simulations. Simulations incorporating full, time-dependent density matrix equations were performed using SIMPSON (*42*) and compiled Matlab codes. These calculations incorporate finite pulses, the magic angle spinning speed, frequency offsets, individual CSA principle values, and relative orientations of the $^{13}C'$ CSAs and the dipolar coupling vector. Fits of the DQ buildup data and 2D DQ evolution data were done iteratively. Initially the distance between the $^{13}C'$ atoms was determined using simulations in which the ϕ and ψ torsion angles were assumed. This distance was used to fit an approximate value for the torsion angle ϕ. This torsion angle was then input with the full range of ψ values (−180°→+180°) into the 2D DQ simulations to find a rough fit of the data. Once these values were known, the DQ buildup data were refit using these torsion angles to orient the CSA and dipolar coupling tensors. This final value of ϕ was then used in setting up the grid of ϕ,ψ torsion angles for the final fit of the 2D DQ data.

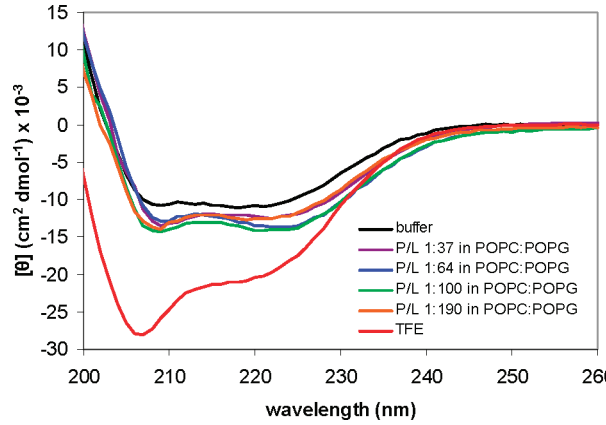

FIGURE 1: CD spectra for KL_4 in buffer, in TFE, and when reconstituted with 3:1 POPC:POPG LUVs, at the concentrations indicated.

RESULTS

CD spectroscopy provides a simple qualitative method for determining peptide secondary structure both in solution and when bound to lipid. As an initial assessment of global secondary structure, CD spectroscopy was performed on KL_4 in 5 mM HEPES at pH 7.4. As shown in Figure 1, the peptide displayed spectral properties that are characteristic of a partially helical structure (Figure 1). Also shown in Figure 1 are CD spectra of KL_4 in 50% TFE and in the presence of 3:1 POPC:POPG LUVs at P/L ratios ranging from 1:35 to 1:200. Helicity can be assessed by examining the ellipticity at 208 and 222 nm; all the spectra showed negative absorption at 208 and 222 nm, indicative of helical secondary structure. Comparison to a spectrum for KL_4 in TFE shows that while the peptide is helical in buffer and when bound to lipid vesicles, it does not display a maximally α-helical signature under these conditions. Fitting of the CD data using standard deconvolution software (*43*) led to secondary structure estimates of 40−60% α-helix, 30−40% random coil, and 10−20% β-sheet.

The conformational stability of KL_4 was analyzed using samples $^{13}C'$-enriched pair wise on adjacent amino acids at positions L2, L3, L4, L5, L7, L8, L9, and L10 (Table 1.) A total of four enriched pairs, L2L3, L4L5, L7L8, and L9L10 were prepared by solid-phase peptide synthetic methods for ssNMR experiments. All samples were characterized using standard ^{13}C CPMAS and $T_{1\rho}$ relaxation (*44*) experiments

Table 1: Peptides Synthesized for NMR Measurements[a]

peptide	isotopic enrichment at C′ position
KL_4-L2, L3	K**LL**LLKLLLLKLLLLKLLLLK
KL_4-L4, L5	KLL**LL**KLLLLKLLLLKLLLLK
KL_4-L7, L8	KLLLLK**LL**LLKLLLLKLLLLK
KL_4- L9,L10	KLLLLKLL**LL**KLLLLKLLLLK

[a] Amino acids indicated in bold are ^{13}C-enriched at the C′ position.

to measure any averaging of ^{13}C′ CSAs, changes in cross polarization efficiencies, or relaxation due to the presence of motion (*45, 46*). CSA and relaxation measurements were performed on all samples under buffered, hydrated conditions as well as after lyophilization. Shown in Figure 2 are CPMAS spectra as a function of the initial peptide:lipid ratio for the KL_4 sample ^{13}C′-enriched at positions L7 and L8 when bound to 3:1 POPC:POPG vesicles and pelleted; the signal intensities are consistent with nearly all of the peptide binding to the lipid vesicles. Spectra are shown for the sample when initially bound to hydrated lipids as well as after freezing and lyophilization. Also shown in Figure 2 are double-quantum filtered spectra of the lyophilized sample demonstrating the simplification of spectra using DQ filtering techniques, allowing easy quantitation of dipolar recoupling data since correction for natural abundance signals is not required. Within the resolution of the CPMAS spectra, a single conformation is observed in all the spectra; no change is observed in the isotropic chemical shifts or the spinning sidebands, indicating that the structure of KL_4 remains constant over the range of peptide:lipid ratios used and only low-amplitude or slow motions occur on the time scale of the experiment. The $T_{1\rho}$ relaxation measurements for these samples also indicate little motion on the kHz time scale (data in Supporting Information). The isotropic and anisotropic chemical shifts for all ^{13}C′-enriched positions are given in Table 2. All leucine positions had similar isotropic chemical shifts and spinning sideband patterns, demonstrating the secondary structure of the bound KL_4 is regular and invariant over peptide:lipid ratios of 1:33 to 1:100 and is not altered by flash freezing and lyophilization. The ^{13}C′ line widths for all samples were 1−2 ppm, values commonly seen for proteins and peptides that are well-structured but not crystalline.

Qualitative information about peptide secondary structure may be inferred by measuring isotropic and anisotropic chemical shifts (*47, 48*). As shown in Figure 2 and given in Table 2, the isotropic ^{13}C′ chemical shifts for both the hydrated and lyophilized samples are near 172 ppm (average η of 0.88). This is a value intermediate between expected chemical shifts for an α-helix (176 ppm) or a β-sheet (170 ppm). Nonetheless, the line widths are consistent with a single conformation and a secondary structure with torsion angles intermediate between a standard β-sheet (−120, 120) or α-helix (−60, −45).

Dipolar recoupling experiments were performed to determine what the high resolution secondary structure of KL_4 is when bound to lipid vesicles. Since ^{13}C CPMAS spectra of KL_4 bound to lipid vesicles contain a significant natural-abundance contribution from the lipids as well as contributions from unenriched positions in the peptide and the NMR probe and rotor materials, quantitative analysis of single quantum spectra is not straightforward. DQDRAWS is an NMR experiment that utilizes DRAWS recoupling to generate double-quantum coherence between two homonuclear spins. Monitoring the generation of the double quantum coherence as a function of mixing time allows determination of the distance between the two spins without have to correct for or make assumptions about natural abundance contributions (*45*). Thus, double-quantum buildup experiments were used to measure the distances between adjacent ^{13}C′ positions in KL_4, stemming from the $1/r^3$ dependence of the dipolar coupling. Previously we have demonstrated this technique can successfully measure internuclear distances in order to determine the torsion angle ϕ over a range of secondary structures with an rmsd of 0.03 Å for distance or 4° for ϕ relative to X-ray structures (*49*). The dipolar recoupling data collected on all four pairs of ^{13}C′ labels are shown in Figure 3 along with simulations that best fit the data. For comparison, simulations for classic secondary structures and a mixture of secondary structures are also given. All the positions monitored were observed to have similar ϕ torsion angles, ranging from −99 to −116, which are intermediate between classic α-helix and β-sheet secondary structures and lie in an energetically favorable region of the Ramachandran plot (*50*). Analyses of the DQ buildup data indicate little or no structural heterogeneity. Simulations of mixtures of α-helix ($\phi = -65$) and β-sheet ($\phi = -120$) were also compared to the experimental data. The simulation for 20% α-helix, 80% β-sheet fit well to the early points for three of the buildup curves, but did not fit well to the later data points (as shown in Figure 3). Additionally, the degree of curvature observed in the data indicates a single dipolar coupling for each sample, consistent with a single conformation. However, determining the overall secondary structure also requires knowledge of the torsion angle ψ.

Once double-quantum coherence is generated, it can then evolve under the influence of the tensor sum of the respective CSAs of the two spins before being converted back to a single quantum state for observation. Since ^{13}C′ spins in peptides possess highly anisotropic CSAs and the relationship of the individual ^{13}C′ CSAs to the peptide amide bonds is well understood, secondary structure can be determined by using this technique to measure the relative orientations of the amide planes. This approach is particularly sensitive for helical structures, where other correlation techniques are less applicable (*49*), with an rmsd of 7° for ψ relative to X-ray structures. Determining ϕ and ψ at this level of accuracy not only yields secondary structure but also gives some indication of helical pitch and long-range order. Two-dimensional DQ correlation spectra were obtained for KL_4 with four samples containing pairs of ^{13}C′ labels, as listed in Table 1, affording both ϕ and ψ torsion angles at several positions along KL_4. Results for KL_4 labeled at positions L9 and L10 are shown in Figure 4 along with a χ^2 analysis of how the data fit simulations with varying ψ torsion angles. Results for all monitored positions are listed in Table 1 and data are available in the Supporting Information. Based on ssNMR measurements alone, the conformation of KL_4 falls into two regimes: one which is helical with ϕ values ranging from −99 to −116 and ψ values ranging from −2 to −58 and a second conformation which is typical of a β-sheet with the same ϕ values and ψ values ranging from +128 to +135. However, the CD data clearly show KL_4 to be partially helical in buffer with increased helicity when interacting with

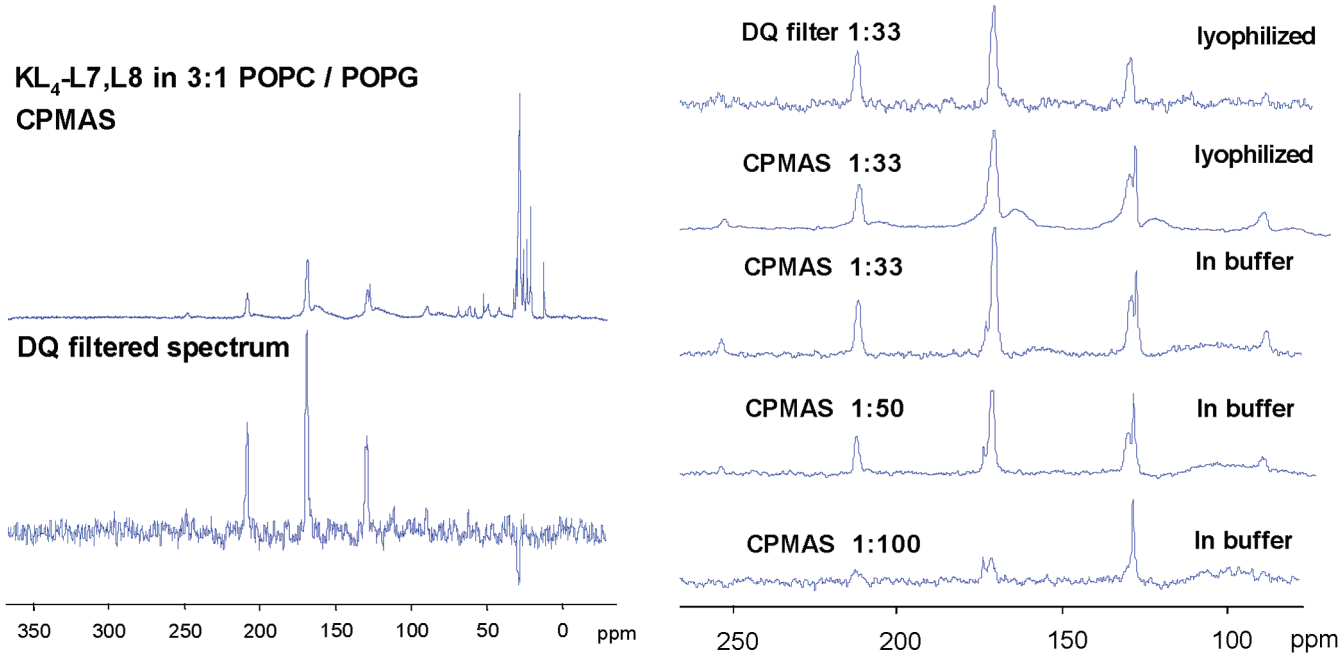

FIGURE 2: CPMAS and DQ-filtered spectra for KL_4 $^{13}C'$-enriched at positions L7 and L8. Left: full ^{13}C CPMAS spectra before and after DQ filtering. Right: expansion of $^{13}C'$ region showing that the peptide chemical shifts are constant over the range of conditions used with NMR experiments, peptide:lipid ratios, and hydration levels as indicated. Also apparent in the unfiltered spectra are the natural abundance contributions from the peptide, lipids, and rotor materials.

Table 2: NMR Results for KL_4 When Interacting with 3:1 POPC:POPG Bilayers

peptide	δ_{iso}[a] (ppm)	δ_{11} (ppm)	δ_{22} (ppm)	δ_{33} (ppm)	$\Delta\sigma$[b] (ppm)	η[c]	distance[d] (Å)	ϕ[e] (deg)	ψ[f] (deg)
KL_4-L2, L3	171.9 (0.1)	244.5 (0.9)	179.5 (1.2)	91.9 (0.3)	152.8	0.81	3.35 (0.02)	−100.5 (1.8)	−17.5 (8.8) 128.0 (3.9)
KL_4-L4, L5	172.1 (0.3)	244.1 (4.2)	176.1 (2.9)	96.1 (4.6)	148.0	0.90	3.46 (0.01)	−115.7 (0.6)	−57.6 (2.9) 135.3 (2.6)
KL_4-L7, L8	171.6 (0.5)	247.4 (2.3)	174.2 (1.4)	93.2 (1.4)	154.2	0.93	3.32 (0.01)	−97.7 (1.3)	−2.5 (6.6) 132.3 (3.1)
KL_4- L9,L10	172.5 (0.5)	248.8 (2.4)	176.8 (0.5)	91.9 (1.9)	156.9	0.89	3.38 (0.01)	−104.4 (0.9)	−41.3 (13.0) 127.1 (3.6)

[a] Chemical shift for two enriched $^{13}C'$ spins, which appear as a single resonance. [b] $\Delta\sigma = \delta_{11} - \delta_{33}$. [c] η as defined by the Haeberlen convention. [d] From DQ buildup experiments. [e] ϕ value determined from DQ buildup distance. [f] Value(s) of ψ determined by fitting 2D DQCSA data with ϕ held to DQ buildup value and ψ freely varied from −180° to +180°. Standard deviations are given in parentheses.

3:1 POPC:POPG LUVs. Thus, the second conformation consistent with the NMR data can be ruled out.

DISCUSSION

For initial structural characterization of lipid-bound KL_4, we have chosen to use 3:1 POPC:POPG vesicles. The composition of lung surfactant lipids consists of 70−80% PC, 10−20% anionic PG and phosphatidylinisotol (PI), and lower levels of sphingomyelin (SM) and phosphatidylethanolamine (PE) (*51*). Approximately 50% of the PC lipids and almost all of the anionic lipids in lung surfactant are monounsaturated. Thus, this lipid composition serves as a reasonable facsimile of bulk lung surfactant and was selected for our structural studies. This composition is also similar to model systems used in many studies of antimicrobial peptides and is convenient for studying peptide/lipid interactions because the T_m for this lipid mixture is well below room temperature.

The sequence of KL_4 is evocative of cationic, leucine-rich amphipathic α-helical peptides which have been pursued as antimicrobial agents since their positive charge leads to their preferential targeting of the anionic rich membranes

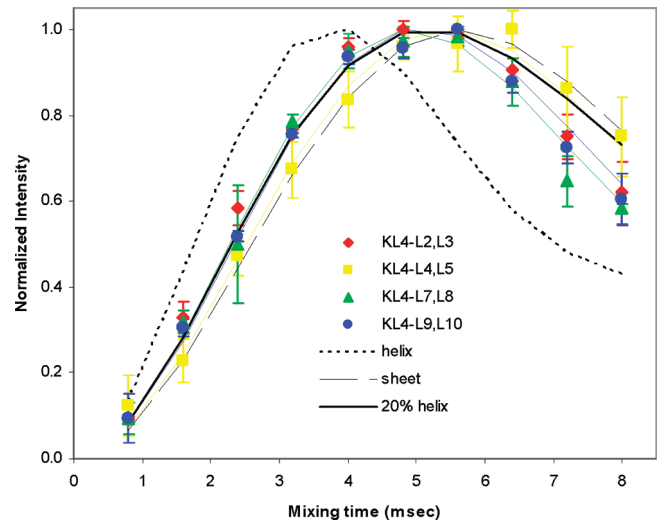

FIGURE 3: DQ buildup data for KL_4 $^{13}C'$-enriched at positions as indicated; error bars represent standard deviation for multiple experiments. Also shown are the best fit simulations of the data as well as for an ideal α-helix, β-sheet, and mixture of helix and sheet.

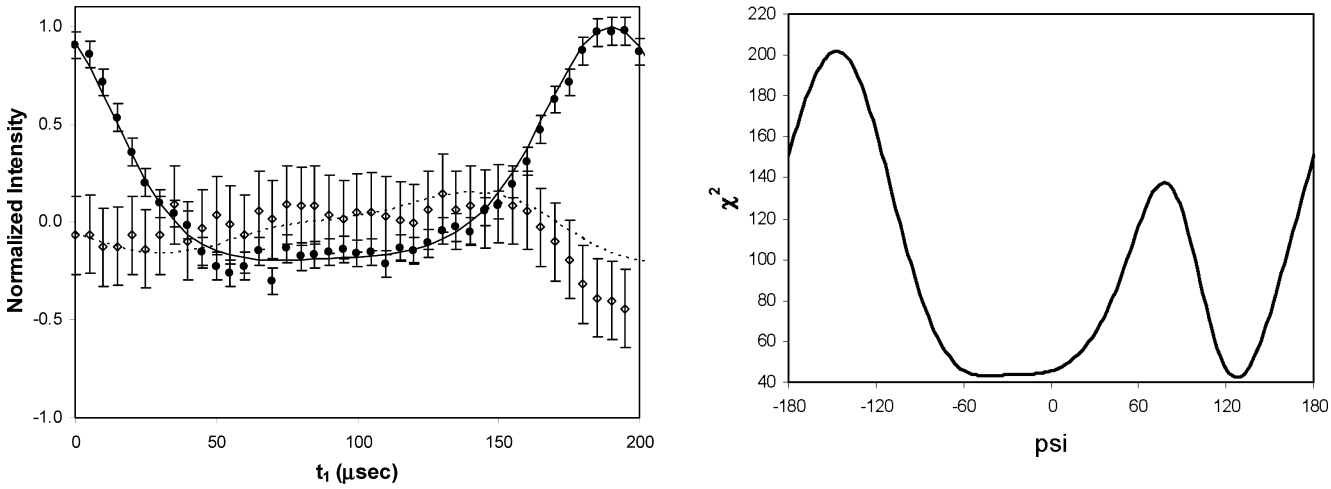

FIGURE 4: Left: 2D-DQ correlation data for KL_4 $^{13}C'$-enriched at positions L9 and L10 along with a best fit simulation. Closed and open symbols are the real and imaginary data points, respectively; solid and dashed lines correspond to the real and imaginary signal trajectories for the best fit (ϕ,ψ) simulation. Error bars represent the standard deviation for multiple experiments. Right: χ^2 evaluation of simulations with varying ψ while holding ϕ at the value obtained from DQ buildup experiments.

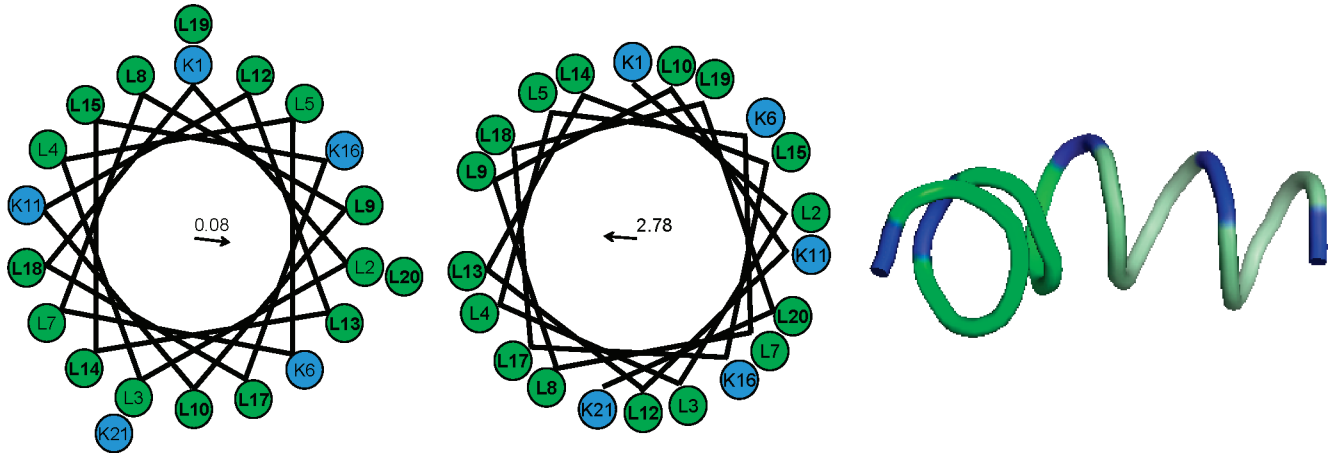

FIGURE 5: Helical wheel representations of KL_4 assuming a classic α-helix (left) and based on ssNMR measurements (middle). Also shown is a ribbon model of KL_4 based on the structural measurements (right). Green residues are leucines directly characterized by ssNMR measurements; blue and light green residues correspond to lysines and leucines, respectively, for which an average backbone conformation of (−105, −30) is assumed.

typical of prokaryotes (*52, 53*). Several synthetic peptides have been designed to be amphipathic α-helices based on naturally occurring antimicrobial peptides and are thought to disrupt the lipid membranes on binding through the formation of toroidal or barrel stave pores structure. In particular, peptides of varying ratios of lysine and leucine residues have been used to modulate peptide helicity and topology in bilayer systems (*54–57*). Specific ratios of L to K that generated a greater hydrophobic face to amphipathic α-helices have been demonstrated to have greater tendency to aggregate, higher lipid affinity, and greater membrane perturbation effects as measured by hemolysis and membrane leakage assays (*55*).

Because KL_4 possesses a sequence that is patterned after the C-terminus of SP-B (*18*), a membrane-bound protein with pronounced helicity (*25*), and since KL_4 is similar in size to antimicrobial peptides that form amphipathic helices when bound to lipids, we would expect the structural properties of KL_4 to be similar. However, as discussed above, FTIR and CD studies of the structure of KL_4 in lipid environments have led to conflicting results regarding the secondary structure and orientation of KL_4 with respect to a lipid bilayer normal (*28–30*), possibly due to differences in lipid composition or due to the dependence of these approaches on assumptions regarding secondary structure as well as the solvation status of the peptide backbone. Also, the distribution of the lysines in KL_4 makes its existence as a canonical α-helix on binding to lipids distinctly unfavorable as it would place the charges evenly around the helix rather than making the helix amphipathic (Figure 5.) Another key feature is that KL_4 has a significantly lower percentage of charged residues (<25% compared to >50% for amphipathic helices commonly studied). The higher hydrophobicity as well as an atypical charge distribution in KL_4 could affect both its structure on lipid binding as well as its effects on lipid phase properties.

Degrado and Lear demonstrated that specific secondary structures could be observed in short peptides at the air/water interface by varying the hydrophobic periodicity in the peptides to match the periodicity of the desired secondary structure (*58*). Previously we ascertained that peptides bearing hydrophobic repeats consistent with α- and 3_{10}-helices were also able to fold into well-defined secondary structures on hydrophobic surfaces (*59*). These and other studies verify that the periodicity of hydrophobic and hydrophilic residues is more important than the helical

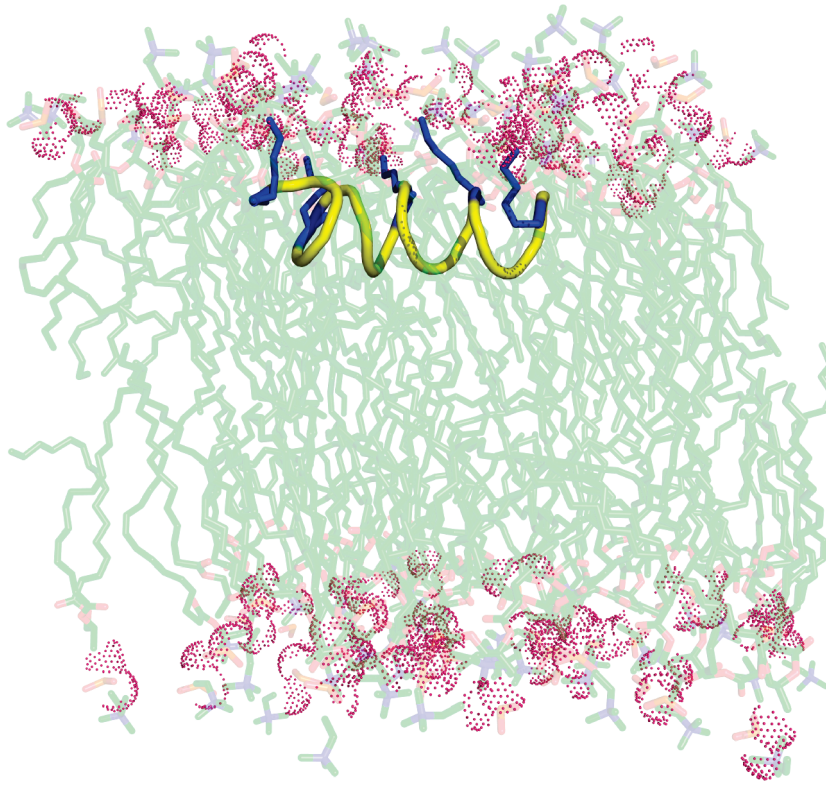

FIGURE 6: Model for the interaction of KL_4 with POPC lipids. Lipid coordinates provided by Scott Fellers, at http://persweb.wabash.edu/facstaff/fellers/ (*71*).

propensity of a particular amino acid in determining peptide secondary structure (*60–65*). This principle should be similar when peptides adsorb and partition into lipid vesicles where the leucine residues have a low partitioning energy and the lysines have one of the higher partitioning energies (*66*).

The ssNMR derived ϕ values determined in our study are not those attributed to a canonical α- helix. However, the ψ values corroborated by the lower resolution CD measurements do lead to (ϕ,ψ) angles in the core helical area of the Ramachandran plot (*50, 67*). It should be noted that deconvolutions of the CD spectra suggest the peptide exists as a mixture of α-helix and random coil while the ssNMR experiments are consistent with a single conformation intermediate between an α-helix and average torsion angles for a random coil. Thus, the lower estimation of helical content based on the CD experiments can be attributed to the basis sets for deconvolution containing only canonical secondary structures; calculations of CD spectra for various helix types support this interpretation (*68*). To better visualize how this backbone secondary structure would affect the placement of the charged lysine sidechains, we generated a structure for KL_4 using the available data and average torsion angles (−105, −30) for positions which were not been monitored in our studies. As can be seen in Figure 5, this generates a peptide structure which is clearly helical. This model is also consistent with intrahelical i→i+4 hydrogen bonds, although work with peptoids as surfactant protein replacements has shown that hydrogen bonding is not critical (*17*). Of particular interest in understanding the role of KL_4 in affecting lipid dynamics, this conformation places the charged lysine residues at positions 6, 11, and 16 on one side of the helix (the ends of the peptide are probably less structured and thus placement of lysines 1 and 21 is less certain). If KL_4 were to partition with its charged lysine residues on a single side and a maximal hydrophobic moment, a π-helix would result. If KL_4 were deeply embedded in the POPC:POPG vesicles, this π-helical structure is reasonable as the charged lysine residues could preferentially interact with the solvent and polar lipid head groups and the leucines are fully partitioned into the lipid acyl chains. However, this type of partitioning requires the bulk of the peptide to be embedded into the acyl chain region which severely limits the dynamics of the acyl chains and might be unfavorable due to the lipids possessing unsaturated fatty acids. Our data show that the structure of KL_4 on binding to monounsaturated lipids is a compromise between adopting a structure with a high hydrophobic moment and maintaining i→i+4 hydrogen bonding leading to a structure and charge distribution that is more favorable for a peripheral location in the lipid bilayers. This structure would allow the mobile lysine side chains to interact with the solvent and polar lipid head groups without requiring a major change in secondary structure from the solution-state favored α-helix. Thus, KL_4 can adapt at the lipid interface with the resulting helix having altered hydrogen bond lengths and orientations relative to classic α-helices.

Based on our structural measurements, a molecular level model for the potential orientation and penetration of KL_4 in POPC:POPG bilayers is shown in Figure 6. Recent work examining the effects of KL_4 on lipid dynamics indicates the lipids remain in a lamellar phase with the peptide at the bilayers interface (unpublished data). For this model, KL_4 was manually docked with the lysine sidechains adopting conformations that maximize interactions with the phosphate headgroups. Given the bilayer thickness and length of the peptide, a transmembrane orientation of the peptide is not likely due to the periodic placement of the lysine residues (*56, 69*); the energetic costs of burying the lysines (particularly lysine

residue 6, 11 and 15) to form a transmembrane helix would be prohibitive since it would involve placement of charged amino acids in a hydrophobic core (*66, 70*).

CONCLUSIONS

Previous work has established that the lung surfactant peptide KL_4 can adopt a helical structure when interacting with lipid assemblies, particularly if anionic and/or monounsaturated lipids are present. Our structural measurements provide the first explanation of how KL_4 forms an amphipathic helix on binding to lipid bilayers. While the peptide is able to form a helix with energetically favorable backbone torsion angles, its structure deviates from that of a canonical α-helix due to the spacing of the charged lysine residues every five amino acids. The implications of this structure on peptide penetration into the lipid bilayers and subsequent effects on lipid properties are the subject of ongoing studies.

ACKNOWLEDGMENT

We thank Professors Art Edison, Gail Fanucci, Manish Mehta, and Adrian Roitberg for helpful discussions. The assistance of Dr. Alfred Chung in peptide synthesis and of the Molecular Structure Facility at University of California, Davis in AAA analysis is gratefully acknowledged. We thank Nathan Oyler for Matlab subroutines used in processing and simulating the NMR data. Numerical simulations were performed at the University of Florida High-Performance Computing Center.

SUPPORTING INFORMATION AVAILABLE

Details of the NMR experiments and numerical simulations as well as data for all the peptides. Pulse sequences (Bruker, Tecmag) and files for simulating 2D DQCSA data with Simpson are available on request (Matlab, c++). This material is available free of charge via the Internet at http://pubs.acs.org.

REFERENCES

1. Goerke, J. (1998) Pulmonary surfactant: functions and molecular composition. *Biochimica Et Biophysica Acta-Molecular Basis of Disease 1408*, 79–89.
2. Piknova, B., Schram, V., and Hall, S. B. (2002) Pulmonary surfactant: phase behavior and function. *Curr. Opin. Struct. Biol. 12*, 487–494.
3. Whitsett, J. A., and Weaver, T. E. (2002) Mechanisms of disease: Hydrophobic surfactant proteins in lung function and disease. *New Engl. J. Med. 347*, 2141–2148.
4. Wright, J. R. (2005) Immunoregulatory functions of surfactant proteins. *Nature Rev. Immunol. 5*, 58–68.
5. Serrano, A. G., and Perez-Gil, J. (2006) Protein-lipid interactions and surface activity in the pulmonary surfactant system. *Chem. Phys. Lipids 141*, 105–118.
6. Clark, J. C., Wert, S. E., Bachurski, C. J., Stahlman, M. T., Stripp, B. R., Weaver, T. E., and Whitsett, J. A. (1995) Targeted disruption of the surfactant protein B gene disrupts surfactant homeostasis, causing respiratory failure in newborn mice. *Proc. Natl. Acad. Sci. U.S.A. 92*, 7794–7798.
7. Ballard, P. L., Nogee, L. M., Beers, M. F., Ballard, R. A., Planer, B. C., Polk, L., deMello, D. E., Moxley, M. A., and Longmore, W. J. (1995) Partial deficiency of surfactant protein B in an infant with chronic lung disease. *Pediatrics 96*, 1046–1052.
8. Clements, J. A., and Avery, M. E. (1998) Lung surfactant and neonatal respiratory distress syndrome. *Am. J. Respir. Crit. Care Med. 157*, S59−66.
9. Revak, S. D., Merritt, T. A., Degryse, E., Stefani, L., Courtney, M., Hallman, M., and Cochrane, C. G. (1988) Use of human surfactant low-molecular weight apoproteins in the reconstitution of surfactant biologic activity. *J. Clin. Invest. 81*, 826–833.
10. Robertson, B., and Halliday, H. L. (1998) Principles of surfactant replacement. *Biochim. Biophys. Acta-Molecular Basis of Disease 1408*, 346–361.
11. Obladen, M. (2005) History of surfactant up to 1980. *Biol Neonate 87*, 308–316.
12. Ghodrat, M. (2006) Lung surfactants. *Am. J. Health Syst. Pharm. 63*, 1504–1521.
13. Johansson, J., and Curstedt, T. (1997) Molecular structures and interactions of pulmonary surfactant components. *Eur. J. Biochem. 244*, 675–693.
14. Weaver, T. E., and Conkright, J. J. (2001) Function of surfactant proteins B and C. *Annu. Rev. Physiol. 63*, 555–578.
15. Robertson, B., Johansson, J., and Curstedt, T. (2000) Synthetic surfactants to treat neonatal lung disease. *Mol. Med. Today 6*, 119–124.
16. Baudouin, S. V. (2004) Exogenous surfactant replacement in ARDS−one day, someday, or never? *N. Engl. J. Med. 351*, 853–855.
17. Seurynck, S. L., Patch, J. A., and Barron, A. E. (2005) Simple, helical peptoid analogs of lung surfactant protein B. *Chem. Biol. 12*, 77–88.
18. Cochrane, C. G., and Revak, S. D. (1991) Pulmonary surfactant protein B (SP-B): structure-function relationships. *Science 254*, 566–568.
19. Cochrane, C. G., Revak, S. D., Merritt, A., Heldt, G. P., Hallman, M., Cunningham, M. D., Easa, D., Pramanik, A., Edwards, D. K., and Alberts, M. S. (1996) The efficacy and safety of KL(4)-surfactant in infants with respiratory distress syndrome. *Am. J. Respir. Crit. Care Med. 153*, 404–410.
20. Cochrane, C. G., Revak, S. D., Merritt, T. A., Schraufstatter, I. U., Hoch, R. C., Henderson, C., Andersson, S., Takamori, H., and Oades, Z. G. (1998) Bronchoalveolar lavage with KL_4-Surfactant in models of meconium aspiration syndrome. *Pediatr. Res. 44*, 705–715.
21. Wiswell, T. E., Smith, R. M., Katz, L. B., Mastroianni, L., Wong, D. Y., Willms, D., Heard, S., Wilson, M., Hite, R. D., Anzueto, A., Revak, S. D., and Cochrane, C. G. (1999) Bronchopulmonary segmental lavage with surfaxin (KL_4-surfactant) for acute respiratory distress syndrome. *Am. J. Respir. Crit. Care Med. 160*, 1188–1195.
22. Sinha, S. K., Lacaze-Masmonteil, T., Soler, A. V. I., Wiswell, T. E., Gadzinowski, J., Hajdu, J., Bernstein, G., d'Agostino, R., and Dist, S. T. A. R. (2005) A multicenter, randomized, controlled trial of lucinactant versus poractant alfa among very premature infants at high risk for respiratory distress syndrome. *Pediatrics 115*, 1030–1038.
23. Cochrane, C. G., and Revak, S. D. (1994) Protein-phospholipid interactions in pulmonary surfactant. The Parker B. Francis Lectureship. *Chest 105*, 57S–62S.
24. Moya, F. R., Gadzinowski, J., Bancalari, E., Salinas, V., Kopelman, B., Bancalari, A., Kornacka, M. K., Merritt, T. A., Segal, R., Schaber, C. J., Tsai, H., Massaro, J., and d'Agostino, R. (2005) A multicenter, randomized, masked, comparison trial of lucinactant, colfosceril palmitate, and beractant for the prevention of respiratory distress syndrome among very preterm infants. *Pediatrics 115*, 1018–1029.
25. Vandenbussche, G., Clercx, A., Clercx, M., Curstedt, T., Johansson, J., Jornvall, H., and Ruysschaert, J. M. (1992) Secondary structure and orientation of the surfactant protein Sp-B in a lipid environment - a Fourier-transform infrared-spectroscopy study. *Biochemistry 31*, 9169–9176.
26. Waring, A. J., Walther, F. J., Gordon, L. M., Hernandez-Juviel, J. M., Hong, T., Sherman, M. A., Alonso, C., Alig, T., Braun, A., Bacon, D., and Zasadzinski, J. A. (2005) The role of charged amphipathic helices in the structure and function of surfactant protein B. *J.Peptide Res. 66*, 364–374.
27. Wustneck, N., Wustneck, R., Perez-Gil, J., and Pison, U. (2003) Effects of oligomerization and secondary structure on the surface behavior of pulmonary surfactant proteins SP-B and SP-C. *Biophys. J. 84*, 1940–1949.
28. Gustafsson, M., Vandenbussche, G., Curstedt, T., Ruysschaert, J. M., and Johansson, J. (1996) The 21-residue surfactant peptide $(LysLeu_4)_4Lys(KL_4)$ is a transmembrane α helix with a mixed nonpolar/polar surface. *FEBS Lett. 384*, 185–188.
29. Cai, P., Flach, C. R., and Mendelsohn, R. (2003) An infrared reflection-absorption spectroscopy study of the secondary structure

in $(KL_4)_4K$, a therapeutic agent for respiratory distress syndrome, in aqueous monolayers with phospholipids. *Biochemistry 42*, 9446–9452.
30. Saenz, A., Canadas, O., Bagatolli, L. A., Johnson, M. E., and Casals, C. (2006) Physical properties and surface activity of surfactant-like membranes containing the cationic and hydrophobic peptide KL4. *FEBS J. 273*, 2515–2527.
31. Tamm, L. K., and Tatulian, S. A. (1997) Infrared spectroscopy of proteins and peptides in lipid bilayers. *Q. Rev. Biophys. 30*, 365–429.
32. Samuel-Landtiser, M., Zachariah, C., Williams, C. R., Edison, A. S., and Long, J. R. (2007) In *Current Protocols in Protein Science* (Coligan, J. E., Dunn, B. M., Speicher, D. W., and Wingfield, P. T., Eds.) Chapter 26, part 3, pp 1–49, John Wiley and Sons, Inc., Brooklyn, NY.
33. Macdonald, R. C., Macdonald, R. I., Menco, B. P. M., Takeshita, K., Subbarao, N. K., and Hu, L. R. (1991) Small-Volume Extrusion Apparatus for Preparation of Large, Unilamellar Vesicles. *Biochim. Biophys. Acta 1061*, 297–303.
34. Gregory, D. M., Mehta, M. A., Shiels, J. C., and Drobny, G. P. (1997) Determination of local structure in solid nucleic acids using double quantum nuclear magnetic resonance spectroscopy. *J. Chem. Phys. 107*, 28–42.
35. Gregory, D. M., Wolfe, G. M., Jarvie, T. P., Sheils, J. C., and Drobny, G. P. (1996) Double-quantum filtering in magic-angle-spinning NMR spectroscopy applied to DNA oligomers. *Mol. Phys. 89*, 1835–1849.
36. Bower, P. V., Oyler, N., Mehta, M. A., Long, J. R., Stayton, P. S., and Drobny, G. P. (1999) Determination of torsion angles in proteins and peptides using solid state NMR. *J. Am. Chem. Soc. 121*, 8373–8375.
37. Stark, R. E., Jelinski, L. W., Ruben, D. J., Torchia, D. A., and Griffin, R. G. (1983) C-13 Chemical-shift and C-13-N-15 dipolar tensors for the peptide-bond in [1-C-13]glycyl[N-15]glycinehydrochloride monohydrate. *J. Magn. Reson. 55*, 266–273.
38. Oas, T. G., Hartzell, C. J., Mcmahon, T. J., Drobny, G. P., and Dahlquist, F. W. (1987) The carbonyl C-13 chemical-shift tensors of 5 peptides determined from N-15 dipole-coupled chemical-shift powder patterns. *J. Am. Chem. Soc. 109*, 5956–5962.
39. Engh, R. A., and Huber, R. (1991) Accurate bond and angle parameters for X-Ray protein-structure refinement. *Acta Crystallogr., Sect. A 47*, 392–400.
40. Teng, Q., Iqbal, M., and Cross, T. A. (1992) Determination of the C-13 chemical-shift and N-14 electric-field gradient tensor orientations with respect to the molecular frame in a polypeptide. *J. Am. Chem. Soc. 114*, 5312–5321.
41. Gabrys, C. M., Yang, J., and Weliky, D. P. (2003) Analysis of local conformation of membrane-bound and polycrystalline peptides by two-dimensional slow-spinning rotor-synchronized MAS exchange spectroscopy. *J. Biomol. NMR 26*, 49–68.
42. Bak, M., Rasmussen, J. T., and Nielsen, N. C. (2000) SIMPSON: A general simulation program for solid-state NMR spectroscopy. *J. Magn. Reson. 147*, 296–330.
43. Andrade, M. A., Chacon, P., Merelo, J. J., and Moran, F. (1993) Evaluation of secondary structure of proteins from UV circular-dichroism spectra using an unsupervised learning neural-network. *Protein Eng. 6*, 383–390.
44. Schaefer, J., Stejskal, E. O., and Buchdahl, R. (1977) Magic-angle C-13 NMR analysis of motion in solid glassy polymers. *Macromolecules 10*, 384–405.
45. Long, J. R., Shaw, W. J., Stayton, P. S., and Drobny, G. P. (2001) Structure and dynamics of hydrated statherin on hydroxyapatite as determined by solid-state NMR. *Biochemistry 40*, 15451–15455.
46. Shaw, W. J., Long, J. R., Campbell, A. A., Stayton, P. S., and Drobny, G. P. (2000) A solid state NMR study of dynamics in a hydrated salivary peptide adsorbed to hydroxyapatite. *J. Am. Chem. Soc. 122*, 7118–7119.
47. Asakawa, N., Kuroki, S., Kurosu, H., Ando, I., Shoji, A., and Ozaki, T. (1992) Hydrogen-bonding effect on C-13 NMR chemical-shifts of L-alanine residue carbonyl carbons of peptides in the solid-state. *J. Am. Chem. Soc. 114*, 3261–3265.
48. Ando, I., Kameda, T., Asakawa, N., Kuroki, S., and Kurosu, H. (1998) Structure of peptides and polypeptides in the solid state as elucidated by NMR chemical shift. *J. Mol. Struct. 441*, 213–230.
49. Mehta, M. A., Eddy, M. T., McNeill, S. A., Mills, F. D., and Long, J. R. (2008) Determination of peptide backbone torsion angles using double-quantum dipolar recoupling solid-state NMR spectroscopy. *J. Am. Chem. Soc. 130*, 2202–2212.
50. Lovell, S. C., Davis, I. W., Adrendall, W. B., de Bakker, P. I. W., Word, J. M., Prisant, M. G., Richardson, J. S., and Richardson, D. C. (2003) Structure validation by C alpha geometry: phi,psi and C beta deviation. *Proteins: Struct., Funct., Genet. 50*, 437–450.
51. Veldhuizen, R., Nag, K., Orgeig, S., and Possmayer, F. (1998) The role of lipids in pulmonary surfactant. *Biochim. Biophys. Acta-Molecular Basis of Disease 1408*, 90–108.
52. Ramamoorthy, A., Thennarasu, S., Lee, D. K., Tan, A., and Maloy, L. (2006) Solid-state NMR investigation of the membrane-disrupting mechanism of antimicrobial peptides MSI-78 and MSI-594 derived from magainin 2 and melittin. *Biophys. J. 91*, 206–216.
53. Hwang, P. M., and Vogel, H. J. (1998) Structure-function relationships of antimicrobial peptides. *Biochem. Cell Biol. 76*, 235–246.
54. Epand, R. F., Lehrer, R. I., Waring, A., Wang, W., Maget-Dana, R., Lelievre, D., and Epand, R. M. (2003) Direct comparison of membrane interactions of model peptides composed of only Leu and Lys residues. *Biopolymers 71*, 2–16.
55. Kiyota, T., Lee, S., and Sugihara, G. (1996) Design and synthesis of amphiphilic α-helical model peptides with systematically varied hydrophobic-hydrophilic balance and their interaction with lipid- and bio-membranes. *Biochemistry 35*, 13196–13204.
56. Strandberg, E., Morein, S., Rijkers, D. T. S., Liskamp, R. M. J., van der Wel, P. C. A., and Killian, J. A. (2002) Lipid dependence of membrane anchoring properties and snorkeling behavior of aromatic and charged residues in transmembrane peptides. *Biochemistry 41*, 7190–7198.
57. Harzer, U., and Bechinger, B. (2000) Alignment of lysine-anchored membrane peptides under conditions of hydrophobic mismatch: A CD,N-15 and P-31 solid-state NMR spectroscopy investigation. *Biochemistry 39*, 13106–13114.
58. Degrado, W. F., and Lear, J. D. (1985) Induction of peptide conformation at apolar water interfaces. 1. A study with model peptides of defined hydrophobic periodicity. *J. Am. Chem. Soc. 107*, 7684–7689.
59. Long, J. R., Oyler, N., Drobny, G. P., and Stayton, P. S. (2002) Assembly of α-helical peptide coatings on hydrophobic surfaces. *J. Am. Chem. Soc. 124*, 6297–6303.
60. Clark, T. D., Buriak, J. M., Kobayashi, K., Isler, M. P., McRee, D. E., and Ghadiri, M. R. (1998) Cylindrical β-sheet peptide assemblies. *J. Am. Chem. Soc. 120*, 8949–8962.
61. Xiong, H. Y., Buckwalter, B. L., Shieh, H. M., and Hecht, M. H. (1995) Periodicity of polar and nonpolar amino-acids is the major determinant of secondary structure in self-assembling oligomeric peptides. *Proc. Natl. Acad. Sci. U.S.A. 92*, 6349–6353.
62. PerezPaya, E., Houghten, R. A., and Blondelle, S. E. (1996) Functionalized protein-like structures from conformationally defined synthetic combinatorial libraries. *J. Biol. Chem. 271*, 4120–4126.
63. Fujita, K., Kimura, S., and Imanishi, Y. (1999) Spherical self-assembly of a synthetic α-helical peptide in water. *Langmuir 15*, 4377–4379.
64. Maget-Dana, R., Lelievre, D., and Brack, A. (1999) Surface active properties of amphiphilic sequential isopeptides: comparison between α-helical and β-sheet conformations. *Biopolymers 49*, 415–423.
65. Powers, E. T., and Kelly, J. W. (2001) Medium-dependent self-assembly of an amphiphilic peptide: direct observation of peptide phase domains at the air-water interface. *J. Am. Chem. Soc. 123*, 775–776.
66. Wimley, W. C., and White, S. H. (1996) Experimentally determined hydrophobicity scale for proteins at membrane interfaces. *Nat. Struct. Biol. 3*, 842–848.
67. Laskowski, R. A., Macarthur, M. W., Moss, D. S., and Thornton, J. M. (1993) Procheck - a program to check the stereochemical quality of protein structures. *J. Appl. Crystallogr. 26*, 283–291.
68. Manning, M. C., and Woody, R. W. (1991) Theoretical CD studies of polypeptide helices - examination of important electronic and geometric factors. *Biopolymers 31*, 569–586.
69. Strandberg, E., and Killian, J. A. (2003) Snorkeling of lysine side chains in transmembrane helices: how easy can it get? *FEBS Lett. 544*, 69–73.
70. Hessa, T., Kim, H., Bihlmaier, K., Lundin, C., Boekel, J., Andersson, H., Nilsson, I., White, S. H., and von Heijne, G. (2005) Recognition of transmembrane helices by the endoplasmic reticulum translocon. *Nature 433*, 377–381.
71. Armen, R. S., Uitto, O. D., and Feller, S. E. (1998) Phospholipid component volumes: determination and application to bilayer structure calculations. *Biophys. J. 75*, 734–744.

BI702551C